

Energy and momentum transfer to a ‘fully-clamped’ elastic plate in an air-blast

Y Yuan and PJ Tan

Department of Mechanical Engineering, University College London,
Torrington Place, London WC1E 7JE, United Kingdom

E-mail: pj.tan@ucl.ac.uk

Abstract. The momentum transfer by a planar wave impinging upon a rigid, free-standing plate in water, a largely incompressible medium, is well understood [1]. Kambouchev et al. [2] extended the results of Taylor [1] to include the nonlinear effects of compressibility whilst Hutchinson [3] has recently addressed the issues of energy and momentum transfer to a rigid, free-standing plate. In this paper, key conclusions from the aforementioned studies are critically re-examined in the context of a ‘fully-clamped’ elastic plate. The dynamic response of an elastic plate is represented by an equivalent single-degree-of-freedom (SDOF) system. A numerical method based on a Lagrangian formulation of the Euler equations of compressible flow and conventional shock-capturing techniques, similar to that employed in [2,3], were employed to solve numerically the interaction between the air blast wave and elastic plate. Particular emphasis is placed on elucidating the energy and momentum transfer to a ‘fully-clamped’ elastic plate compared to its rigid, free-standing counterpart, and on whether enhancement in the beneficial effects of FSI as a result of fluid compressibility remains and to what extent.

1. Introduction

Over the past decade, there have been renewed interests in understanding how fluid structure interaction (FSI) in a compressible medium may be exploited to design lightweight sandwich panels with better blast amelioration capabilities. To this end, Kambouchev et al. [2] and Hutchinson [3] have carried out detailed numerical studies to quantify the effects of nonlinear compressibility upon the energy and momentum transfer to plates subjected to air blast loading. However, their findings apply only to rigid, free-standing plates. Recent studies in [4–6] used a single-degree-of-freedom (SDOF) representation to study the effects of mass, time ratio (period of the pressure pulse to the natural period of vibration of the structure) and velocity ratio (shock front velocity to the maximum velocity acquired by the structure) upon the maximum deflection of a flexible structure. However, none have addressed the important issue of energy and momentum transfer, and/or the effects of boundary conditions.

In this paper, the numerical method in [2,3] is employed to study the fluid structure interaction between an air blast wave and a ‘fully clamped’ elastic plate. The emphasis is on comparing the energy and momentum transfer to a ‘fully-clamped’ elastic plate with its rigid, free-standing



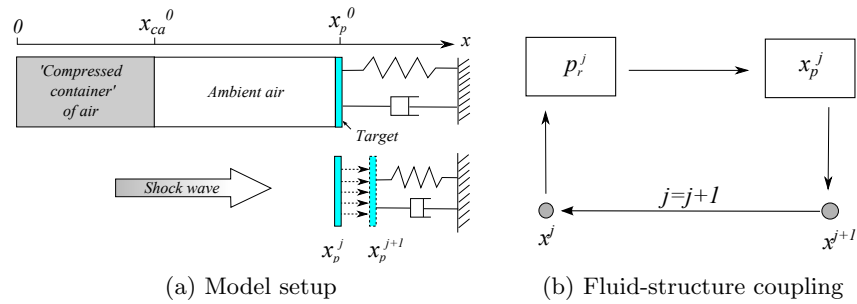


Figure 1. Schematic of model set-up and fluid-structure coupling strategy.

counterpart. Also investigated in this paper is whether enhancement in the beneficial effects of FSI, as a result of fluid compressibility, also applies to a non-free-standing, i.e. supported, structure and to what extent. The results reported here is part of an on-going study to model the influence of boundary conditions upon the momentum and energy transfer to deformable (elasto-plastic) plates through FSI to be published elsewhere.

2. Shock wave generation and its interaction with an elastic plate

Consider a one-dimensional (1D) ‘air-column’ of two parts, viz. ‘compressed container’ of isentropic air and quiescent ambient air, and a flexible elastic plate which is represented by an equivalent SDOF system as shown in Fig. 1a. At time $t = 0$ the ‘compressed container’ of air in the interval $0 \leq x \leq x_{ca}^0$ is prescribed with an initial velocity distribution of

$$v(x) = v_0 e^{-(x/x_{ca}^0)^2}, \quad (1)$$

where x is the Lagrangian coordinate. It follows immediately that the compressed air has a density distribution $\rho(x)$ and a finite initial energy per unit area ΔE_0 given by [3]

$$\begin{aligned} \left[\frac{\rho(x)}{\rho_a} \right]^\gamma &= \left[1 + \frac{\gamma-1}{2} \left(\frac{v(x)}{c_a} \right)^2 \right]^{\gamma/(\gamma-1)} \\ \Delta E_0 &= \frac{p_a x_{ca}^0}{\gamma-1} \left[\left(1 + \frac{\gamma-1}{2} \left(\frac{v_0}{c_a} \right)^2 \right)^{\gamma/(\gamma-1)} - \left(1 + \frac{\gamma-1}{2} \left(\frac{v_0}{c_a} \right)^2 \right)^{1/(\gamma-1)} \right] \end{aligned} \quad (2)$$

where $\gamma (= 1.4)$ is the ratio of specific heats, $p_a (= 104761 \text{ Pa})$ is pressure, $\rho_a (= 1.225 \text{ kg/m}^3)$ is air density, $c_a (= 346 \text{ m/s})$ is speed of sound in air and the subscript ‘a’ denotes ambient conditions. At time $t = 0$, the compressed air is suddenly released into the quiescent ambient air which generates a pressure pulse reminiscent of those in an explosive detonation; this same technique is also employed in [3].

By way of an example, consider a fluid domain of length $d = 10 \text{ m}$ and a ‘compressed container’ of length $x_{ca}^0 = 0.5 \text{ m}$. The 1D domain is discretised using a uniform grid of 2000 nodes and the classical Euler equations of compressible flow are solved explicitly by finite difference, see [2]. Artificial viscosity was introduced to smooth the shock discontinuities but in a manner that still preserves energy conservation [3]. The time step was chosen to ensure it satisfies the stability requirement of the iterations. Figure 2a shows the displacement of 100 nodes and the ‘shock locus’ generated by the travelling wave. Note the dash lines represent the motion of the ‘compressed container’. The incident and reflected pressure-time history following wave

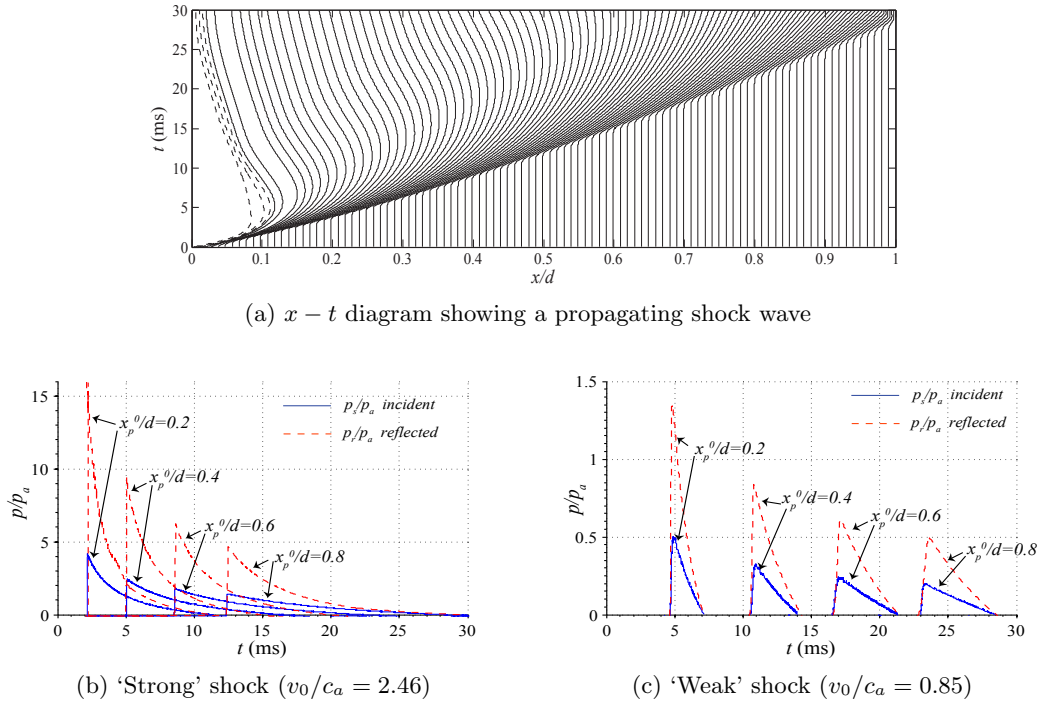


Figure 2. (a) Shock wave generated by ‘compressed container’ method and (b,c) incident and reflected pressure-time histories upon interaction with a massive rigid wall at different standoff.

interaction with a massive rigid wall of infinite mass at different standoff are compared in Figs. 2b and 2c for different blast intensities. The intensity of the blast wave is controlled by the non-dimensional parameter v_0/c_a . Some key observations can be made as follows: (1) nonlinear compressibility causes the peak of the evolving pulse to decrease, with a corresponding increase in pulse duration, with distance travelled; (2) the ratio of the peak reflected to incident pressure is between 2 to 8 as predicted by the well-known Rankine-Hugoniot relationships; and (3) the incident and reflected impulse is identical at different standoff since the artificial viscosity was set to preserve energy conservation, i.e. the wave generated is essentially isentropic. In order to ensure that the plate remains elastic, i.e. deforming in Mode I [7], a relatively ‘weak’ shock of $v_0/c_a = 0.85$ is used in subsequent simulations.

The equation of motion of the elastic plate, represented by an equivalent SDOF system with stiffness k_e and damping coefficient c_e , both per unit area, is given by

$$m_e \ddot{x}_p + c_e \dot{x}_p + k_e x_p = F_e(t) \quad (3)$$

where $(\dot{}) \equiv d()/dt$, x_p is displacement, m_e is equivalent mass per unit area and $F_e (= p_r K_L)$ is equivalent load per unit area. The damping coefficient c_e is given by $c_e = \alpha(\rho_a c_a)$, where α is chosen to reflect the severity of structural damping. The equivalent values were derived following the procedure outlined by Biggs [8]. Table 1 list the properties of two aluminium plates, of identical mass per unit area, but different flexural rigidity per unit length. Implementation of fluid structure coupling is achieved by solving for the interface pressure (reflected pressure p_r^j) and plate displacement x_p^j which are updated at every time step as shown schematically in Fig. 1b.

Table 1. Properties of square aluminium plates and equivalent parameters of SDOF model.

Parameters	Symbol	Plate-1	Plate-2
Density (kg/m ³)	ρ_p	2760	2760
Young's modulus (GPa)	E	69	69
Poisson's ratio	ν	0.33	0.33
Dimensions (m)	$a \times b \times h$	$4 \times 4 \times 0.0275$	$2 \times 2 \times 0.0275$
Second moment of area (m ⁴) [8]	$I_a = ah^3/12$	6.93×10^{-6}	3.47×10^{-6}
Flexural rigidity/length (kNm) [8]	$D = EI_a/b$	119.58	119.58
Mass factor [8]	K_M	0.21	0.21
Load factor [8]	K_L	0.33	0.33
Equivalent stiffness/area (kN/m ³) [8]	$k_e = K_L \frac{810D}{a^4}$	124.86	1997.8
Equivalent mass/area (kg/m ²) [8]	$m_e = K_M \rho_p h$	15.94	15.94
Natural period (ms)	T	71.0	17.7

3. Results and Discussions

To check that the SDOF model is correctly implemented and gives sensible predictions, the reflected over-pressure for the 'weak' shock case, shown in Fig. 2c, is prescribed as a stand-alone pressure loading to the fully-validated FE model in [7] and to the SDOF model, both in an uncoupled manner from the fluid domain. Note that damping is initially ignored. Figure 3a shows excellent agreement between the predicted maximum displacement x_p by the uncoupled SDOF model and the maximum central deflection of its equivalent square plate in the uncoupled FE model.

Parametric studies carried out in [4, 6] have established that FSI has the beneficial effects of reducing the maximum displacement of flexible structure. In Fig. 3a, the predictions by both the coupled and uncoupled SDOF model show that increasing standoff reduces the maximum displacement although this effect is more apparent with FSI. This is because the plate experiences a shorter overall loading duration as a result of the coupling which is evident in Fig. 3b. On the other hand, increasing the equivalent plate stiffness per unit area at a given standoff distance does not appear to offer any significant advantage in terms of the maximum plate deflection.

Figure 4 compares the momentum and energy transfer to free-standing (of infinite flexural rigidity) and fully-clamped plates (of two different flexural rigidity given in Table 1). The ratio of transmitted impulse I_p to incident impulse $I_0 (= \int_0^{t_d} p dt)$ is plotted in Fig. 4a. As expected, the rigid free-standing plate acquires a higher momentum (or transmitted impulse) compared to its fully-clamped counterpart. What is surprising, however, is that the plate with a higher flexural rigidity appears to acquire a slightly lower impulse. The total energy E_T transferred to the plate is dissipated as kinetic energy E_K by the free-standing plate and as kinetic E_K plus strain E_S energies by its fully-clamped counterpart shown in Fig. 4b. Since the rigid free-standing plate is free to displace, a greater amount of energy $E_T = \int_0^{x_p} p_r dx_p$ is transmitted compared to its fully-clamped, flexible counterpart as shown in Fig. 4b. Previous studies on the effects of FSI for free-standing plate have shown that a smaller plate mass displaces further, thus relieving the incident pressure acting on the plate [2, 3, 9]. Figure 4c plots the non-dimensional transmitted impulse vs. FSI index ($\beta_s = \rho_s U_s t_0 / m_e$ where ρ_s is density of gas behind shock front, U_s is shock speed, t_0 is the duration of an equivalent uniform shock and m_e is equivalent mass per unit area). β_s was introduced in [2, 9] to take into account nonlinear compressibility effects. The results in Fig. 4c agrees with those in previous studies where the transmitted impulse is

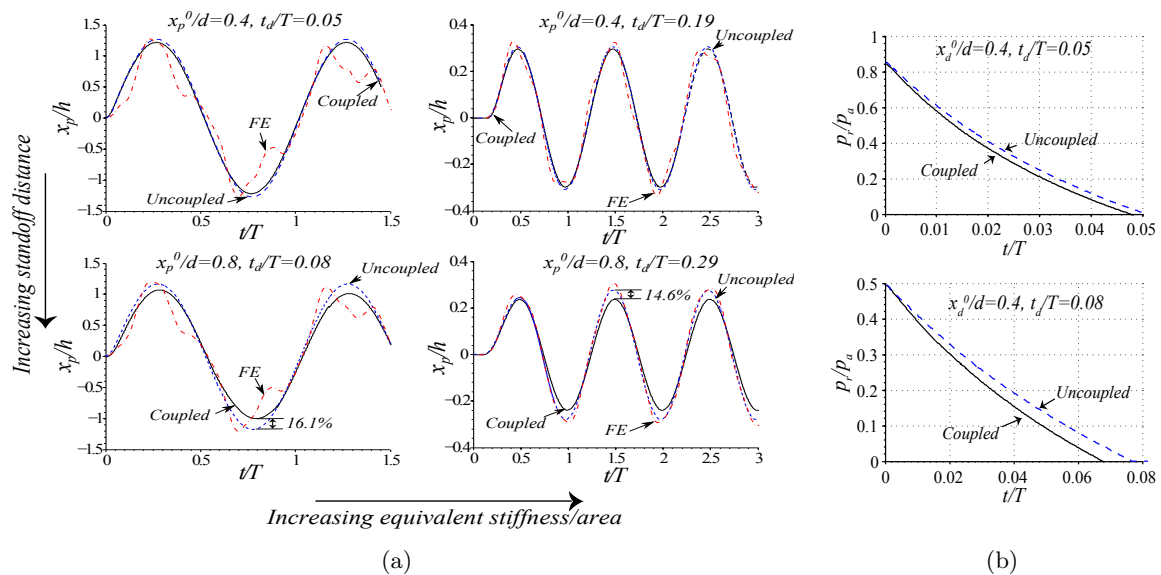


Figure 3. (a) Predicted displacement histories without damping and (b) ratio of the normalised reflected pressure p_r/p_a versus t/T for Plate 1. Coupled SDOF model (—) ; uncoupled SDOF model (---) ; uncoupled FE predictions (-.-.).

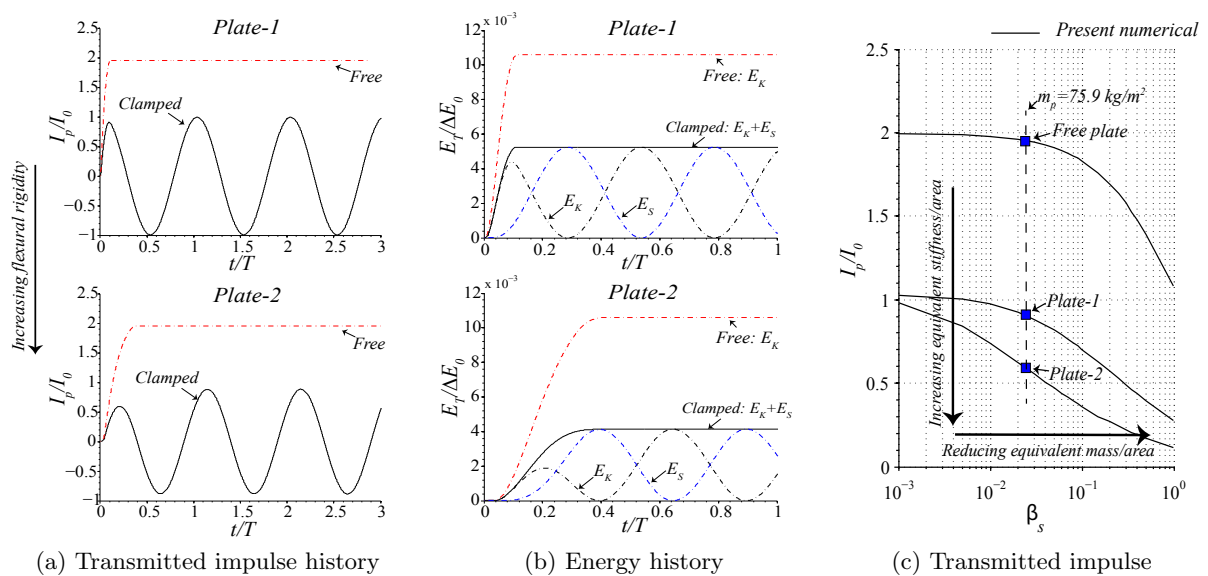


Figure 4. Comparison of momentum and energy transfer to a free-standing and its corresponding fully-clamped plate.

observed to increase with β_s . By contrast, the restraint offered by a clamped boundary leads to a significant reduction in the impulse transmitted to the plate for a given β_s . Therefore, the introduction of a clamped boundary appears to further enhance the beneficial effects of FSI. The implication is that a structure with a higher equivalent stiffness and/or a smaller equivalent mass, both per unit area, acquires less impulse and energy in an air blast.

Lastly, the effects of structural damping is shown in Fig. 5. The results show that greater

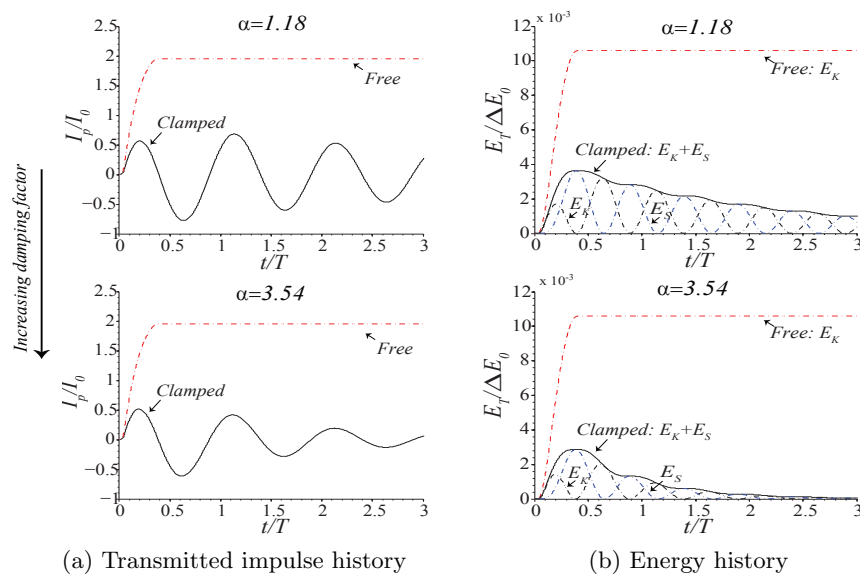


Figure 5. The effects of damping upon the momentum and energy transfer for Plate-2.

damping, i.e. a higher α , leads to greater beneficial effects of FSI in terms of the momentum and energy transferred to the structure. This is because the damping force always opposes the direction of motion and this further contributes to the beneficial effects of FSI.

4. Conclusion

Fluid structure interaction between an air blast wave and a fully-clamped elastic plate is studied. Three important conclusions can be drawn:

- The resistance to transverse displacement, offered by a lateral restraint in the form of a support, further enhances the beneficial effects of FSI.
- Higher structural damping also improves the beneficial effects of FSI.
- Stiff and light structures minimise the impulse and energy transmitted in an air blast.

References

- [1] Taylor G I 1963 *The Scientific Papers of Sir Geoffrey Ingram Taylor* **3** 287–303
- [2] Kambouchev N, Noels L and Radovitzky R 2006 *J App Phys* **100** 063519
- [3] Hutchinson J W 2009 *J App Mech* **76** 051307
- [4] Subramaniam V K, Nian W and Andreopoulos Y 2009 *Int J Impact Eng* **36** 965–974
- [5] Rigby S, Tyas A and Bennett T 2012 *Eng Structures* **45** 396 – 404
- [6] Teich M and Gebbeken N 2011 *Eng Structures*
- [7] Yuan Y and Tan P J 2013 *Int J Impact Eng* **59** 46 – 59
- [8] Biggs J 1964 *Introduction to structural dynamics* (New York: McGraw-hill)
- [9] Kambouchev N, Noels L and Radovitzky R 2007 *Computers & Structures* **85** 923–931